Toughening of Thermosets by the Creation of Residual Compressive Stresses

Ho Sung Kim, Nam Ho Kim

Discipline of Mechanical Engineering, School of Engineering, Faculty of Engineering and Built Environment, University of Newcastle, Callaghan, NSW 2308, Australia

Received 27 July 2005; accepted 14 September 2005
DOI 10.1002/app.23235
Published online in Wiley InterScience (www.interscience.wiley.com).

ABSTRACT: The toughening of thermosets through the creation of residual compressive stresses around microspheres was studied. Expandable, hollow microspheres containing gas with heating were used for the creation of residual compressive stresses. Microscopic compressive residual stresses in the vicinity of the crack tip were graphically analyzed and related to the macroscopic mechanical behavior for mode I fracture. The graphical analysis and experimental results confirmed that toughening was achieved mainly because of residual compressive stresses rather than a postcure effect. As expected, however, no toughening effect was found in mode III fracture. © 2006 Wiley Periodicals, Inc. J Appl Polym Sci 100: 4045–4051, 2006

Key words: electron microscopy; fracture; mechanical properties; thermosets; toughness

INTRODUCTION

Toughness is one of the important mechanical properties in structural applications of thermosets and has been an issue for improvement since the 1970s.[1,2] A toughening method involves adding second-phase particles to the resin matrix.[3–8] In traditional rubber toughening, rubber/matrix cavitation and shear yielding between rubber particles have been identified as dominant toughening mechanisms.[8,9] Recently, Kim and Kim[10–14] developed a new toughening method using expandable, hollow microspheres containing liquefied gas. The method involves the production of residual compressive stresses around dispersed microspheres, which expand on heating, and hence increases the effective stress intensity factor at fracture. They provided photoelastic fringe patterns around hollow microspheres as evidence for the residual stresses. However, one could argue that the photoelastic fringe patterns could be caused by molecular reorientation only without much stress.[15] As such, the possibility that the improvement is due to a postcure effect with heat treatment rather than residual stress can be raised.

In this article, further analysis and results from our previous work[12] are presented to support the previous claim that the toughness improvement is due predominantly to compressive residual stresses around microspheres, and we further determine the relationship between the microscopic compressive residual stresses around the microspheres in the vicinity of the crack tip and the macroscopic mechanical behavior. Also, mode III fracture behavior is studied to provide further insight into the toughening mechanism.

GRAPHICAL ANALYSIS OF THE EFFECT OF THE RESIDUAL COMPRESSIVE STRESSES AROUND MICROSPHERES ON THE MECHANICAL BEHAVIOR OF A LINEAR, ELASTIC, CRACKED SOLID FOR MODE I

The nonlinearity of a stress–strain trace is caused by the material properties, a transition from elastic deformation to plastic deformation, and/or a large change in the configuration of the specimen.[16] The same applies to a stress intensity/displacement (SD) trace. The stress intensity in the case of a cracked body is quantified by the stress intensity factor for mode I (K_I). The SD trace is linear for linear, elastic solids (before gross plastic deformation). When a cracked solid contains residual compressive stresses around microspheres, as illustrated in Figure 1, however, the residual compressive stresses also affect the SD trace and then manifest as nonlinearity. The reason is that, as the applied load increases, the residual compressive stresses in the vicinity of the crack tip decrease, finally disappear if they are sufficiently close to the crack tip, and then are replaced by increasing tensile stresses until the specimen fails.

Correspondence to: H. S. Kim (ho-sung.kim@newcastle.edu.au).

Contract grant sponsor: University of Newcastle Postgraduate Research Scholarship (to N.H.K.).
Contract grant sponsor: University of Newcastle (through a Research Grants Committee project grant).

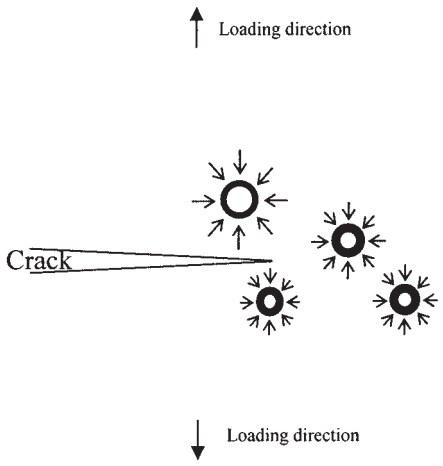

Figure 1 Residual compressive stresses around microspheres in the vicinity of the crack tip before loading.

The stresses can be graphically analyzed, as shown in Figure 2. Figure 2(a) illustrates both the tensile stress and residual compressive stress components at a point near a hollow microsphere; they both linearly increase with the same slope (if the moduli for compression and tension are equal) as the applied load increases. When the two stress components are superimposed, the linearity of the trace [Fig. 2(a)] is lost, as shown in Figure 2(b). The initial residual compressive stress, shown in Figure 2(a), contributes to the increase in the effective stress intensity [Fig. 2(b)]. The slope in Figure 2(a) varies with the location of the point for consideration. The arrow in Figure 2(b) indicates the transition at which no residual compressive stress remains, and only tensile stress starts to increase at the point. The transition from compressive stress to tensile stress takes place progressively from one point to another because of the nonuniform stress distribution around the crack tip. As a result, K_I, which represents the whole area near the crack tip, becomes a curve, as shown in Figure 2(c). Moreover, some residual compressive stresses around microspheres in some other parts of the specimen do not completely disappear because (1) the tensile stresses are not sufficiently strong to offset the compressive

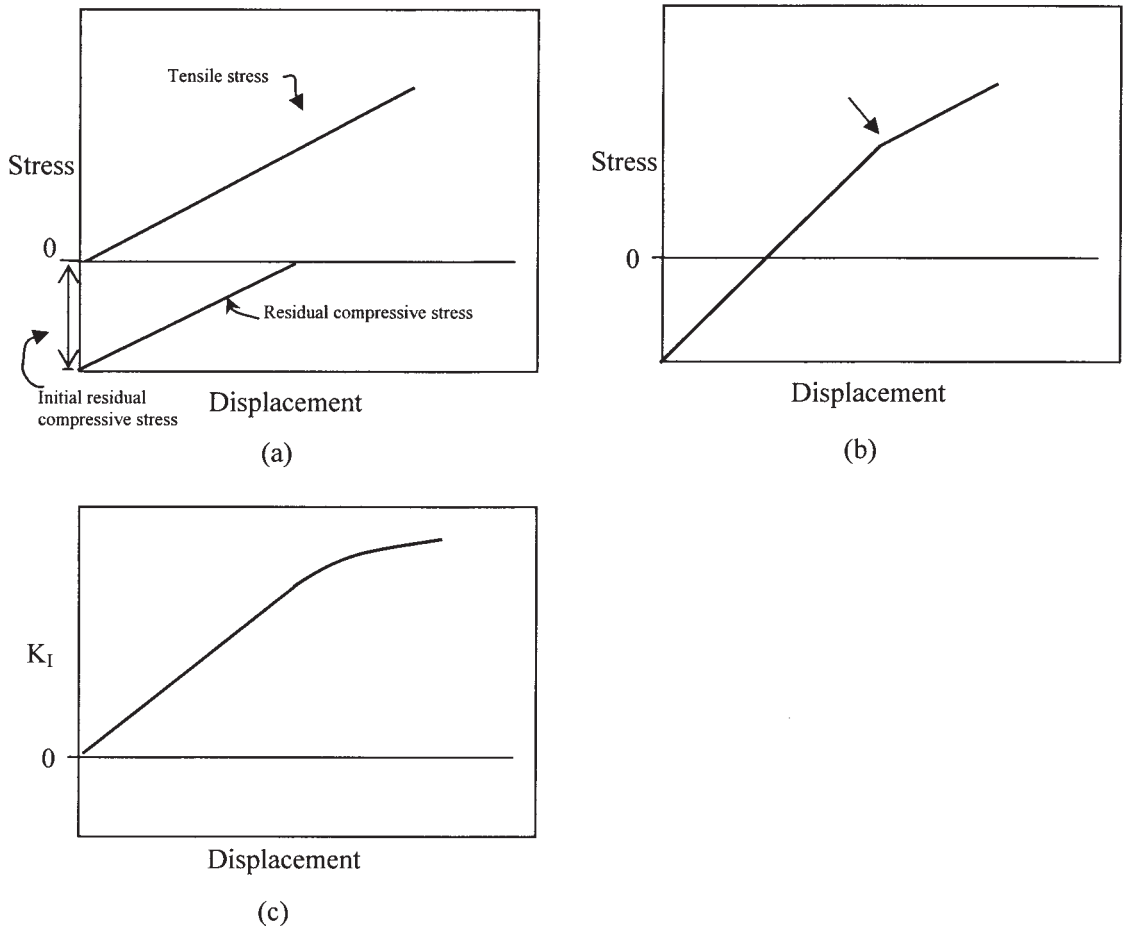

Figure 2 Stress components at a point near a hollow microsphere in the vicinity of the crack: (a) stress before superposition, (b) stress after superposition, and (c) K_I.

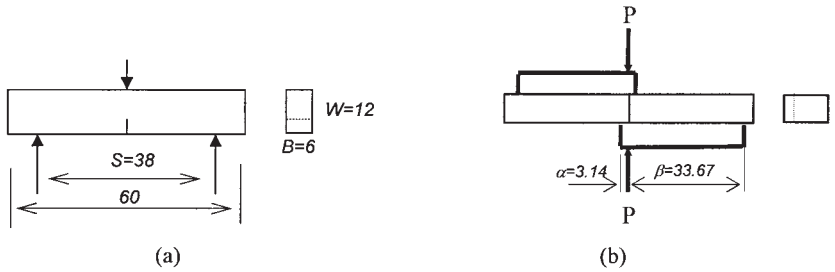

Figure 3 Mechanical testing configurations: (a) three-point loading for both flexural and mode I fracture tests but without the notch for flexural tests and (b) four-point, skew-symmetric loading for mode III fracture tests. All dimensions are in millimeters.

stresses and (2) the tensile stress direction is not always triaxial.

EXPERIMENTAL

Materials

An epoxy system was adopted as a model material for this study. The system consisted of West System Epoxy 105 (a blend of bisphenol A and bisphenol F) and West System Slow Hardener 206 (a blend of aliphatic amines and aliphatic amine adducts based on diethylene triamine and triethylene tetramine) (West System, Bay City, MI) as curing agents. An average density of five measurements was found to be 1.1 for the epoxy system.

The modifiers were hollow microspheres (Expancel, 551 DU40, Akzo Nobel; Sundsvall, Sweden), which consisted of a copolymer shell and gas (isobutane). The average density of the microspheres from three measurements at room temperature was found, with a Beckman 930 air comparison pycnometer (Seattle, WA), to be 1.2. The microspheres expanded when heated.

Preparation of the test specimens

Two series of specimens for microsphere modification were prepared: one without heat treatment (ME) and the other with heat treatment (MEH).

The mixing of the control epoxy and curing agent in a bowl was conducted by manual stirring for 5 min. The amount of the curing agent was 17 phr (by weight) for all specimens. The resulting mixture was poured into an aluminum mold with a 6-mm-thick cavity and left to cure at room temperature at least for 1 day. A temperature rise in the mold due to an exothermic reaction was monitored with a thermocouple and found to be about 8°C, which did not affect the expansion temperature (ca. 90°C) of the hollow microspheres. The exothermic temperature rise depended on the mold size and material.

For both ME and MEH, various amounts (by mass) of 551 DU40 were added to epoxy and stirred manually for about 10 min. The mixtures were heated to about 80°C (which was lower than the microsphere expanding temperature) for 30 min to reduce the viscosity for easy stirring and then allowed to cool gradually in a water bath for about a half-hour. The hardener was then added and stirred for 5 min. The casting and curing were conducted in the same way as for the control epoxy system.

The heat treatment was conducted for all the cured specimens of MEH in an oven at 135°C for 2 h, which were then allowed to cool to room temperature. The heat treatment was used to produce residual compressive stresses and strains around the microspheres, as already demonstrated in refs. 11 and 12.

Mechanical testing

The testing specimens for the elastic modulus (E), flexural strength (σ_y), and mode I fracture were machined into dimensions of 12 × 60 × 6 mm; for mode III fracture, the dimensions were 12 × 1000 × 6 mm. Three-point-bending tests on a Shimadzu 5000 universal testing machine (Kyoto, Japan) were conducted for E, σ_y, and the mode I fracture toughness. Mechanical testing configurations are shown in Figure 3. A crosshead speed of 10 mm/min was adopted for tests of the flexural properties, and a crosshead speed of 0.5 mm/min was adopted for both mode I and mode III fracture tests at room temperature (21°C).

E and σ_y were calculated with the following equations given in ASTM D 790M-93:

$$E = \frac{S^3 m}{4BW^3} \tag{1}$$

$$\sigma_y = \frac{3PS}{2BW^2} \tag{2}$$

where S is the support span, B is the thickness, W is the width, m is the slope of the tangent to the initial

TABLE I
Mechanical Properties of the ME and MEH Epoxy Systems

Expancel (phr)	G_{IC} (kJ/m^2)		σ_y (MPa)		E (GPa)	
	ME	MEH	ME	MEH	ME	MEH
0	0.31	0.64	130.65	131.04	1.42	1.50
5		1.61		116.08		1.25
10	1.06	1.96	67.16	102.52	1.60	1.11
15		2.61		90.27		1.10
20	1.99	4.29	62.24	34.78	1.21	0.85
25		2.89		43.36		0.95
30	1.59	3.89	63.34	24.67	1.07	0.69
35		3.31		29.74		0.67
40	1.80	3.30	62.53	29.22	1.09	0.65
45		3.36		23.28		0.56
50	1.08	2.89	55.20	22.58	0.92	0.54

straight-line portion of the load–deflection curve, and P is the load.

The critical stress intensity factor expression for mode I (K_{IC})[17] was

$$K_{IC} = \frac{3P_c S\sqrt{\pi a}}{2BW^2} Y \tag{3}$$

where a is the crack length, P_c is the load at fracture, and Y is a geometry factor given by

$$Y = \frac{1}{\sqrt{\pi}} \frac{1.99 - \frac{a}{W}\left(1 - \frac{a}{W}\right)\left[2.15 - 3.93\frac{a}{W} + 2.7\left(\frac{a}{W}\right)^2\right]}{\left(1 + 2\frac{a}{W}\right)\left(1 - \frac{a}{W}\right)^{3/2}} \tag{4}$$

The specific fracture energy values for mode I (G_{IC}) were approximated with

$$G_{IC} = \frac{K_{IC}^2}{E} \tag{5}$$

The critical stress intensity factor expression for mode III (K_{IIIC})[17] was

$$K_{IIIC} = \tau Y_3 \sqrt{\pi a} \tag{6}$$

where τ is given by

$$\tau = \frac{P_c(\beta - \alpha)/(\alpha + \beta)}{WB} \tag{7}$$

and Y_3 is a geometry factor given by

$$Y_3 = \sqrt{\frac{2w}{\pi a} \tan\left(\frac{\pi a}{2w}\right)} \tag{8}$$

A precrack, 3–5 mm long, was produced by a razor blade being tapped into the tip of a saw-cut notch, 2 mm long, of each fracture test specimen, and its length was measured with a pair of Vernier calipers.

Microscopy

Scanning electron microscopy (SEM) work (Oxford-XL30, Philips) was conducted for specimens coated with gold. The specimens were cleaned with water with a Bran Sonic 52 (Danbury, CT) and dried in an oven at 30°C for 30 min before coating for SEM.

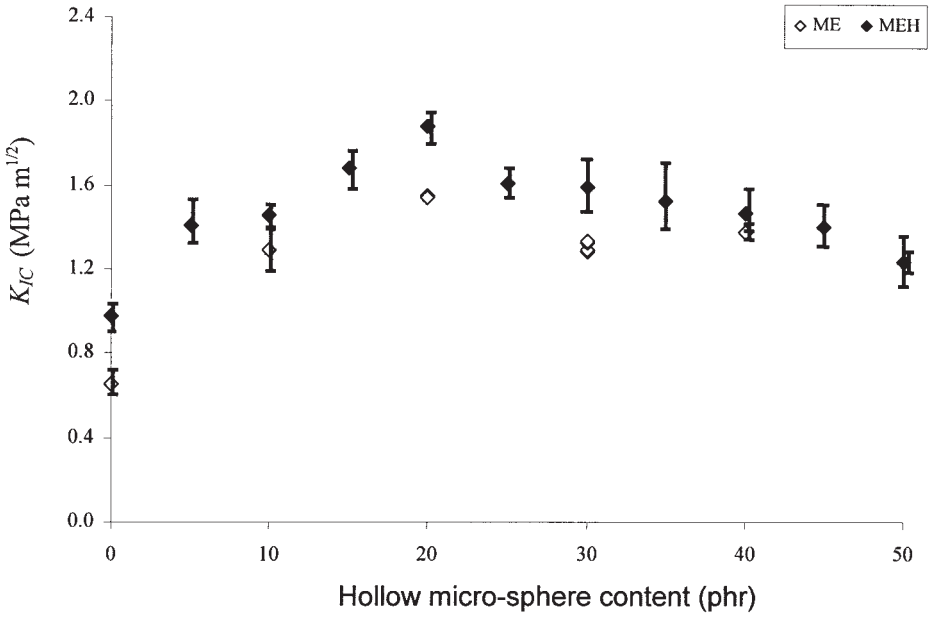

Figure 4 K_{IC} as a function of the hollow microsphere content for the ME and MEH series.

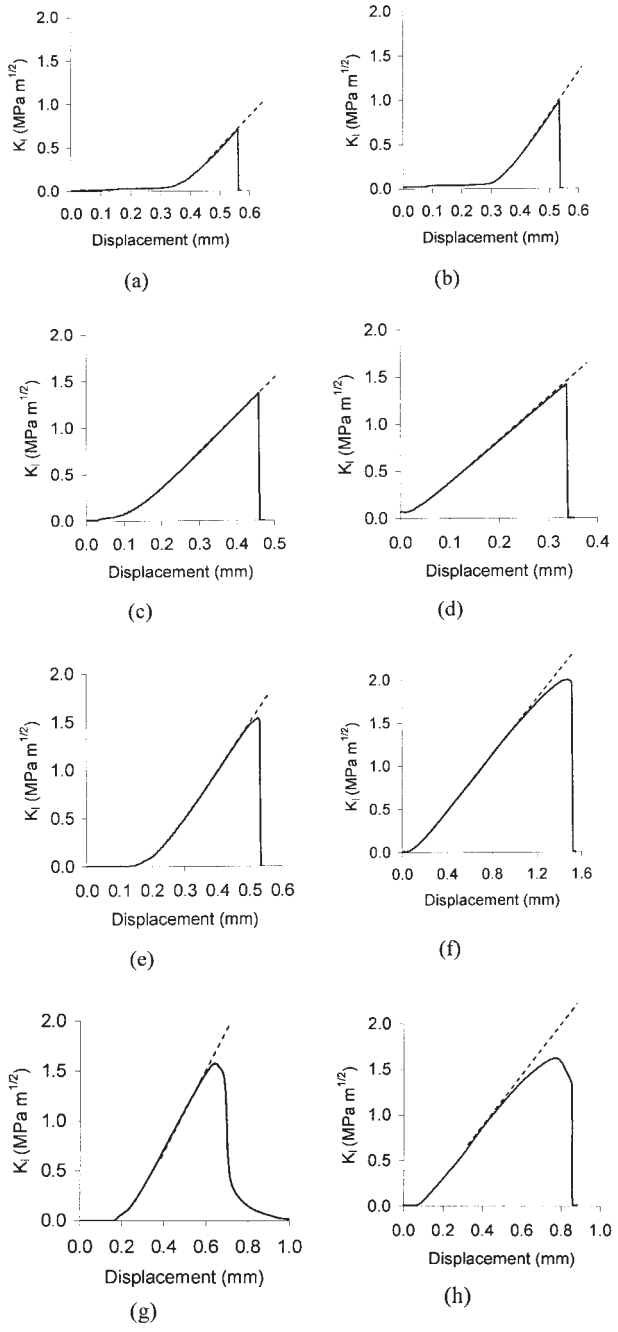

Figure 5 K_I versus d: (a) control ME, (b) control MEH, (c) 10 phr ME, (d) 10 phr MEH, (e) 20 phr ME, (f) 20 phr MEH, (g) 30 phr ME, and (h) 30 phr MEH. Straight, dashed lines have been added for the detection of nonlinearity.

RESULTS AND DISCUSSION

Some mechanical properties for both the ME and MEH series are given in Table I. As already discussed in our previous work,[12] specimens of the ME series were identified to be toughened dominantly by cavitation, whereas those of MEH were claimed to be toughened dominantly by residual compressive stresses in the absence of cavitation. Also, K_{IC} is plotted as a function of the hollow microsphere content in Figure 4. The toughness of MEH is generally higher than that of ME, and this implies that toughening by residual compressive stress is more efficient than that by cavitation. The SD traces as a function of the displacement (d) for various hollow microsphere contents are given in Figure 5 to test the hypothesis that the toughening in MEH is due mainly to the residual compressive stresses.

The initial positive $\partial^2 K_I/\partial d^2$ value on each curve in Figure 5 is due obviously to the adjustment of loose mechanical joints. As the hollow microsphere content increases, the nonlinearity appears prominent. Let us consider control epoxy systems first. They, for both ME and MEH, behave linearly [Fig. 5(a,b), respectively]. The heat treatment (or postcure) does not alter the linearity, even though it appears to contribute to the toughness improvement of the control epoxy system (Fig. 4). The linearity experienced in the control epoxy systems is still maintained at a hollow microsphere content of 10 phr for both ME and MEH in this particular case [Fig. 5(c,d), respectively]. However, part of the linearity begins to be replaced with nonlinearity at a point for both ME and MEH at 20 phr [Fig. 5(e,f), respectively]. In the case of ME [Fig. 5(e)], the nonlinearity is due mainly to plasticity because, as already discussed elsewhere,[12] the toughening is dominantly due to cavitation rather than residual compressive stress. In the case of MEH [Fig. 5(f)], though, the nonlinearity should be due mainly to the residual compressive stress because the toughening is achieved not only in the absence of cavitation but also with strong photoelastic evidence of residual stress/strain around microspheres. As already demonstrated elsewhere,[13,14] the residual compressive stress reduces even existing cavitation/shear banding (i.e., plastic deformation). Also, no macroscopic plastic deformation of broken specimens was visually detectable. (It was too difficult to stop loading and unload at the right moment to demonstrate elasticity because of the small ranges of d from three-point test specimens.) One could still argue that photoelastic evidence for the residual compressive stress is not sufficient because it reflects only molecular chain reorientation (which is

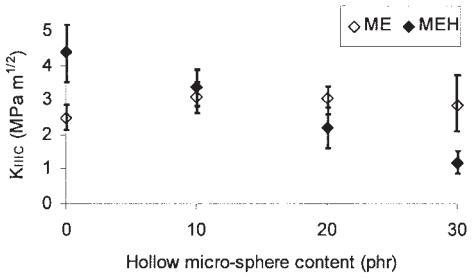

Figure 6 K_{IIIC} versus the hollow microsphere content for ME and MEH.

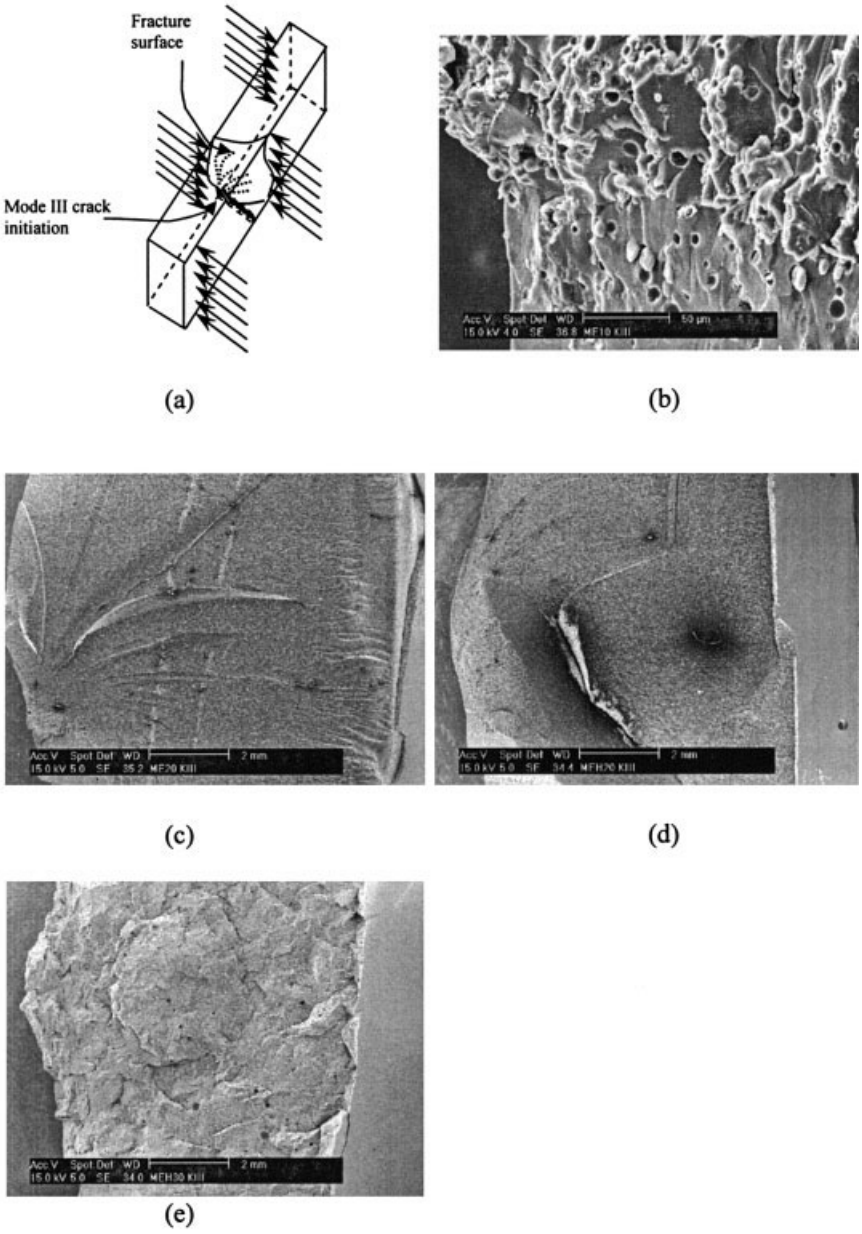

Figure 7 Mode III fracture: (a) a sketch indicating the relative SEM locations in a test specimen for the following SEM fracture surfaces, (b) a crack initiation site of 10 phr ME at a high magnification, (d) a fracture surface of 20 phr ME, (d) a fracture surface of 20 phr MEH, and (e) a fracture surface of 30 phr MEH. The crack initiation site is located at the bottom, left-hand corner of each SEM fracture surface.

strain but not necessarily stress). Therefore, the nonlinearity cannot be caused only by residual compressive strain without residual compressive stress, as graphically analyzed and discussed earlier. Thus the facts along with this discussion sufficiently support the hypothesis that the toughening in MEH is due mainly to the residual compressive stress. Furthermore, negative $\partial K_I/\partial d$ values after the peak in the MEH series begin to appear at 20 phr [Fig. 5(f)] and are prominent at 30 phr [Fig. 5(h)]. Such a transition is possibly due to a geometry change due to internal cracking, which is discussed later.

The stress components in the x, y, and z directions around the crack tip (σ_x, σ_y, and σ_z, respectively) are 0 for mode III loading according to the theoretical stress analysis.[18] However, necessary conditions for toughening by either cavitation or residual compressive stress are $\sigma_x > 0$, $\sigma_y > 0$ and $\sigma_z > 0$. It is thus expected that none of those toughening mechanisms will occur under mode III loading. If the MEH series were toughened by a postcure effect when heat-treated, it might be toughened. K_{IIIC}, measured for both ME and MEH, has been plotted as a function of the hollow microsphere content in Figure 6. The toughness of the ME

series indeed displays no substantial increase over the control, and that of the MEH series even decreases as the hollow microsphere content increases. The decrease in MEH seems to be due to some internal cracking, which was found later. The internal cracking was observed at 20 phr or higher in the MEH series. A concentration of 20 phr appears to be a transitional point because internal cracking was not always found on cross sections of specimens. Some SEM images are given in Figure 7. Figure 7(a) illustrates the locations of mode III crack initiation and fracture surfaces with respect to the mode III loading for the images in Figure 7(b–e). Figure 7(b) shows the mode III crack initiation site of an ME specimen with a hollow microsphere content of 10 phr. Only some microspheres in the lower part of the image are partially sheared from left to right. It is difficult to achieve pure mode III fracture entirely because mode III fracture tends to be mode I ultimately.[19,20] Figure 7(c,d) shows fracture surfaces of ME and MEH, respectively, for 20 phr microspheres at a low magnification. A major difference between ME and MEH appears to be due to the influence of internal cracking on the fracture surface. More influence of internal cracking is noticed on the fracture surface of the MEH specimen with a microsphere content of 30 phr [Fig. 7(e)]; marks of chipping rather than propagation can be seen. Thus, the toughness decrease in MEH seems to reflect the internal cracking.

CONCLUSIONS

Toughening for thermosets associated with residual compressive stress under mode I loading has been studied with expandable, hollow microspheres containing liquefied gas as modifiers. The effect of the presence of residual compressive stresses around microspheres on macroscopic mechanical behavior has been established. Graphical analysis together with our previous microscopic evidence[12] confirms that the toughening effect achieved in heat-treated modified epoxy systems (MEH) is due mainly to residual compressive stresses rather than a postcure effect.

Mode III fracture behavior has also been studied. No substantial toughening was observed in the case of the ME series, and the toughness of the MEH series even decreased as the modifier content increased.

The authors thank Ted Kuc of International Sales and Marketing Pty., Ltd., for providing Expancel 551 DU40, D. Phelan of the Em/X-ray unit for assisting with scanning electron microscopy, and Bale Richard of the Department of Geology for assisting with transmission optical microscopy.

References

1. Sultan, J. N.; McGarry, F. J. Polym Eng Sci 1973, 13, 29.
2. Bucknall, C. B. Toughened Plastics; Applied Science: London, 1977; Chapter 1.
3. Pearson, R. A.; Yee, A. F. Polymer 1993, 34, 3658.
4. Garg, A. C.; Mai, Y.-W. Compos Sci Technol 1988, 31, 179.
5. Huang, Y.; Hunston, D. L.; Kinloch, A. J.; Riew, C. K. In Toughened Plastics I: Science and Engineering; Riew, C. K.; Kinloch, A. J., Eds.; Advances in Chemistry Series 233; American Chemical Society: Washington, DC, 1993; p 1.
6. Kim, H. S.; Ma, P. J Appl Polym Sci 1998, 69, 405.
7. Pearson, R. A.; Yee, A. F. J Mater Sci 1986, 21, 2475.
8. Kunz-Douglass, S.; Beaumont, P. W. R.; Ashby, M. F. J Mater Sci 1980, 15, 1109.
9. Bagheri, R.; Pearson, R. A. Polymer 1996, 37, 4529.
10. Kim, H. S.; Kim, N. H. Int. Pat. WO 2004/003069 A1 (2004).
11. Kim, N. H.; Kim, H. S. Annu Tech Conf 2003, 2, 2069.
12. Kim, N. H.; Kim, H. S. J Appl Polym Sci 2005, 98, 1663.
13. Kim, N. H.; Kim, H. S. Proceedings of the 5th International Conference on Composite Science and Technology, Sharjah, United Arab Emirates, Feb 2005; p 149.
14. Kim, N. H.; Kim, H. S. J Appl Polym Sci, to appear.
15. Schiraldi, D. Personal communication, Case Western Reserve University, Cleveland, OH, March 2005.
16. Elber, W. Damage Tolerance in Aircraft Structures; ASTM STP 486; American Society for Testing and Materials: West Conshohocken, PA, 1971; p 230.
17. Tada, H.; Paris, P. C.; Irwin, G. R. The Stress Analysis of Cracks Handbook, 2nd ed.; Paris Productions: St. Louis, 1985.
18. Paris, P. C.; Sih, G. C. Fracture Toughness Testing and Its Applications; ASTM STP 381; American Society for Testing and Materials: West Conshohocken, PA, 1964; p 30.
19. Kim, H. S.; Karger-Kocsis, J. Acta Mater 2004, 52, 3123.
20. Kim, H. S.; Karger-Kocsis, J. Proceedings of the 4th Australasian Congress on Applied Mechanics, Melbourne, Australia, 2005; p 365.